Performance Limitations of Air Flow Control in Power-Autonomous Fuel Cell Systems

Kyung-Won Suh and Anna G. Stefanopoulou

***Abstract*—We quantify here the performance limitations of a proton exchange membrane fuel cell with a compressor-driven air supply under transient loading conditions. We first model and analyze the dynamics of the fuel cell system equipped with a compressor, which for power autonomy must be powered by the fuel cell itself. Experimental data are used to qualitatively verify the fuel cell system model. Several control architectures for regulating oxygen into the fuel cell stack are proposed to demonstrate the limitations both analytically and through simulations.**

***Index Terms*—Feedback control, feedforward control, fuel cells, integral relations, nonminimum phase.**

I. Introduction

GIVEN the importance of responding to fast changing and unpredictable electric loads, fuel cell systems need to satisfy strict transient performance requirements. A prompt response is also essential for autonomy and driveability in fuel cell power automotive propulsion or in portable auxiliary power units. One key factor in transient response is controlling the air supply and avoiding oxygen starvation, particularly in the proton exchange membrane (PEM) fuel cell fed by compressed high-purity hydrogen. In such a system, oxygen is supplied through the air supply system and it is typically forced by a blower or a compressor. Although the compressor absorbs a significant amount of power and increases the fuel cell parasitic losses, it is preferred to a blower due to the higher achievable power density (kW/m^3). A blower is typically not capable of pushing high flow rates through the small channels associated with high power density fuel cell (FC) stacks. An analysis of the tradeoff between FC power density and parasitic losses from the air supply device can be found in [1].

When operating under low air flow to minimize parasitic loss associated with powering the flow device, PEM fuel cells are prone to partial oxidant starvation during dynamic load changes even with an optimized flow field design. This temporary low oxidant stoichiometry produces a cell voltage drop, resulting in a local temperature increase. A further problem is that insufficient gas flow associated with dynamic load may cause an accumulation of excess water, which can possibly block reactant diffusion. Anomalous operating conditions such as these can lead to a decrease in performance, which may be reversed, or possibly to irreversible degradation. Therefore, understanding the limits of our ability to control the air flow in a PEM fuel cell stack is of considerable importance.

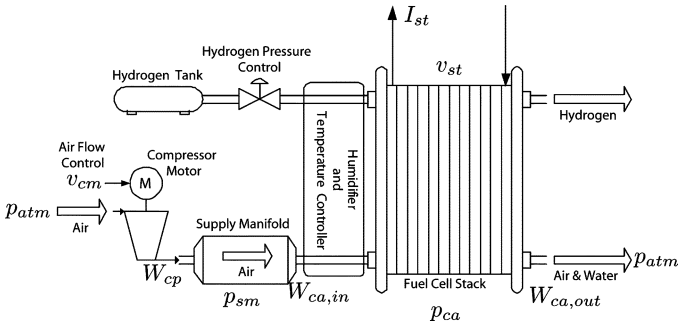

Fig. 1. FC reactants supply system.

The goal of this brief is to examine the performance limitations and tradeoffs associated with the compressor-driven air supply shown in Fig. 1, which for power autonomy, needs to be powered from the fuel cell. Regulating oxygen concentration in the FC stack based on the measured compressor flow rate poses a challenge because the actual air flow at the stack inlet and at the compressor outlet differ [2]–[4]. More importantly, a high compressor control effort to move air quickly into the stack can cause instabilities when the compressor draws current directly from the stack [5]. The tradeoff between satisfying net power requirements and maintaining the optimum air supply in the stack during load changes was first defined in [6]. We show here that this difficulty is more critical when the compressor motor draws its power directly from the fuel cell as in the case of an autonomous fuel cell. The control limitations in achieving fast air flow control in the stack is the result of two nonminimum phase zeros in the air supply control system. We clarify and quantify these limitations and design controllers that illustrate these limitations in simulations.

The analysis of performance limitations is based on a low-order FC model described in Section II. Comparison between the experimental data and the model simulation is also presented in this section. In Section III, the physical problem is formulated. The performance measures and control difficulty are summarized in Section IV. In Section V, we discuss various feedforward control architectures based on load current measurement and compare them both analytically and with simulation. The feedback controller design based on air flow measurement is presented in Section VI.

II. Power-Autonomous FC System

In a high pressure PEM FC system, a compressor supplies the air flow necessary for the reaction, which depends on the current drawn from the FC, $I_{\rm st}$, as shown in Fig. 1. The air supplied

Manuscript received May 27, 2006; revised November 7, 2006. Manuscript received in final form January 29, 2007. Recommended by Associate Editor U. Christen. This work was supported in part by the National Science Foundation under 0201332 and the Automotive Research Center (ARC) under U.S. Army Contract DAAE07-98-3-0022.

K.-W. Suh is at the Advanced Technology Center, Hyundai Motor Company, Gyeonggi 449-912, Korea (e-mail: kwsuh@hyundai-motor.com).

A. G. Stefanopoulou is with the Department of Mechanical Engineering, University of Michigan, Ann Arbor, MI 48109 USA (e-mail: annastef@umich.edu).

Color versions of Figs. 3–8 are available online at http://ieeexplore.ieee.org.

Digital Object Identifier 10.1109/TCST.2007.894640

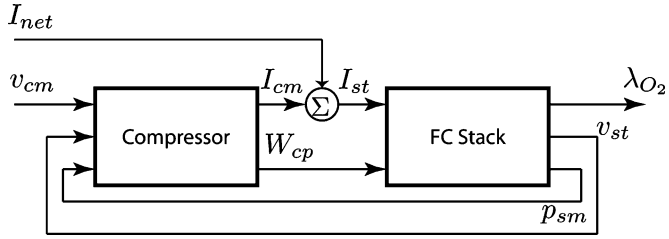

Fig. 2. Interaction between the air compressor and the FC variable in a power-autonomous FC stack system.

to the cathode should exceed the air necessary for reaction for several reasons [7], [8]. The oxygen excess ratio (OER), defined as λ_{O_2} in (2) of Section II-A, is a convenient lumped variable that defines the control objective in the FC air supply. Regulation of λ_{O_2} to a high value can provide enough oxygen into the FC stack to prevent oxygen starvation, but the overall efficiency may decrease due to power losses in the air compressor. In this study, we consider the air flow control problem associated with regulating the oxygen excess ratio at a fixed desired value ($\lambda_{\mathrm{O}_2}^{\mathrm{ref}} = 2$), which has been shown to provide an adequate supply of oxygen and optimum power generation in the FC stack in [3]. We consider the regulation problem where the compressor is driven directly by the FC. The total current drawn from the FC stack, I_{st} is defined as the sum of the net current I_{net}, which is the current delivered to the load, and the current drawn by all of the FC auxiliaries, particularly the compressor load, I_{cm}

$$I_{\mathrm{st}} = I_{\mathrm{net}} + I_{\mathrm{cm}} = I_{\mathrm{net}} + \frac{P_{\mathrm{cm}}}{v_{\mathrm{st}}} = I_{\mathrm{net}} + \frac{v_{\mathrm{cm}}(v_{\mathrm{cm}} - k_v\omega_{\mathrm{cp}})}{R_{\mathrm{cm}}v_{\mathrm{st}}} \quad (1)$$

as shown in the signal flow diagram in Fig. 2. Here, the power required to drive the compressor motor is considered to be the largest contributor to FC parasitic losses through the power drawn from the motor P_{cm} directly from the stack bus.[1] To calculate the current consumed by the compressor, we assume that the compressor motor has an ideal power converter approximated with a compressor resistant R_{cm}. The compressor motor supplies the necessary power P_{cm} drawn at the FC stack bus voltage v_{st}, as dictated by the dc motor control signal v_{cm} and the compressor speed ω_{cp} defined later in (6).

The compressor motor current I_{cm} and power P_{cm} are, thus, simply instantaneously drawn from the stack through a dc motor control unit. Through this coupling, the FC air supply interacts with the FC stack through both an electrical and an air flow path, as shown in Fig. 2. The electrical coupling is established by the stack voltage v_{st} through (1). The FC stack voltage v_{st} is given by a polarization relation in [3] and [8], which mainly depends on the stack current I_{st}. The air flow through the compressor depends on the FC stack supply manifold pressure p_{sm}, as will be shown later in Section II-A. As can be seen in Fig. 2, the effect of the compressor voltage command v_{cm} on the oxygen excess ratio λ_{O_2} is also influenced by the interaction between the compressor and the FC stack through the air flow path and the electrical path.

[1]A 75-kW FC stack is typically supplied by 15-kW compressor power [3], [9].

A. FC System Model

We consider an FC stack with an active cell area of $A_{\mathrm{fc}} = 280\,\mathrm{cm}^2$ and $n = 381$ number of cells with 75-kW gross power output that is appropriate for automotive or residential use. We assume a compressed hydrogen supply, shown in Fig. 1, that simplifies the anode reactant flow. The cooler and humidifier are ignored in this study because they consume less power than the compressor [10]. The performance variable is the oxygen excess ratio λ_{O_2} in the cathode that indirectly ensures adequate oxygen supply to the stack

$$\lambda_{\mathrm{O}_2} = \frac{W_{O_2,\mathrm{in}}}{W_{O_2,\mathrm{rct}}} \quad (2)$$

where the rate of oxygen reacting in the cathode is $W_{O_2,\mathrm{rct}} = M_{\mathrm{O}_2}(nI_{\mathrm{st}}/4F)$ with the molar mass of oxygen M_{O_2} and the Faraday number F, and the oxygen supplied $W_{O_2,\mathrm{in}} = (x_{O_2,\mathrm{atm}}/1 + w_{\mathrm{atm}})W_{\mathrm{ca,in}}$ depends on oxygen mass fraction x_{O_2}, the atmospheric humidity ratio w_{atm}, and on the total flow in the cathode $W_{\mathrm{ca}} = k_{\mathrm{ca,in}}(p_{\mathrm{sm}} - p_{\mathrm{ca}})$, which depends on the difference between the supply manifold pressure p_{sm} and the cathode pressure p_{ca}, which is the sum of the oxygen pressure p_{O_2}, nitrogen pressure p_{N_2}, and vapor partial pressure p_{sat}. The oxygen excess ratio is typically regulated at $\lambda_{\mathrm{O}_2}^{\mathrm{ref}} = 2$ to reduce the formation of stagnant vapor and nitrogen films in the electrochemical area. Values of λ_{O_2} lower than 1 indicate oxygen starvation, which has serious consequences for the stack life.

The dynamic behavior of the variables associated with the air flow control, namely, oxygen pressure p_{O_2}, total cathode pressure p_{ca}, and supply manifold pressure p_{sm}, can be predicted [3], [8] by applying the mass continuity of the oxygen and nitrogen inside the cathode volume and ideal gas law

$$\frac{dp_{\mathrm{O}_2}}{dt} = \frac{\bar{R}T_{\mathrm{st}}}{M_{\mathrm{O}_2}V_{\mathrm{ca}}}\left(W_{O_2,\mathrm{in}} - W_{O_2,\mathrm{out}} - W_{O_2,\mathrm{rct}}\right) \quad (3)$$

$$\frac{dp_{N_2}}{dt} = \frac{\bar{R}T_{\mathrm{st}}}{M_{N_2}V_{\mathrm{ca}}}\left(W_{N_2,\mathrm{in}} - W_{N_2,\mathrm{out}}\right) \quad (4)$$

where V_{ca} is the lumped volume of the cathode, $\bar{R}$ is the universal gas constant, and M_{N_2} is the molar mass of nitrogen. The inlet mass flow rate of nitrogen $W_{N_2,\mathrm{in}}$ can be calculated from the inlet cathode flow, $W_{N_2,\mathrm{in}} = ((1 - x_{O_2,\mathrm{atm}})/(1 + w_{\mathrm{atm}}))W_{\mathrm{ca,in}}$. The outflow $W_{(\cdot),\mathrm{out}}$ in (3) and (4) is calculated similarly to the inflows $W_{(\cdot),\mathrm{in}}$ with the total flow rate at the cathode exit $W_{\mathrm{ca,out}}$ which is calculated by the nozzle flow equation because the pressure difference between the cathode and the ambient pressure is large in pressurized stacks [3].

The supply manifold model describes the mass flow rate from the compressor to the outlet mass flow. The rate of change in air pressure in the supply manifold that connects the compressor with the FC (shown in Fig. 1) depends on the compressor flow into the supply manifold W_{cp}, the flow out of the supply manifold into the cathode $W_{\mathrm{ca,in}}$ and the compressor flow temperature T_{cp}

$$\frac{dp_{\mathrm{sm}}}{dt} = \frac{\bar{R}T_{\mathrm{cp}}}{M_{a,\mathrm{atm}}V_{\mathrm{sm}}}(W_{\mathrm{cp}} - W_{\mathrm{ca,in}}) \quad (5)$$

where $V_{\rm sm}$ is the supply manifold volume and $M_{a,\rm atm}$ is the molar mass of atmospheric air.

Finally, the compressor flow $W_{\rm cp}$ is modeled by applying the Jensen and Kristensen nonlinear fitting method [3] as functions of the pressure ratio $p_{\rm sm}/p_{\rm atm}$, the upstream temperature $T_{\rm atm}$, and the compressor rotational speed $\omega_{\rm cp}$, which is calculated through Newton's law

$$\frac{d\omega_{\rm cp}}{dt} = \frac{1}{J_{\rm cp}}(\tau_{\rm cm} - \tau_{\rm cp}) \tag{6}$$

where $\tau_{\rm cm} = P_{\rm cm}/\omega_{\rm cp}$ is the compressor motor torque and $\tau_{\rm cp}$ is the load torque of the compressor defined by employing adiabatic assumptions [3]. Note again that the compressor power P_{cm} modeled as in (1) is supplied directly from the FC instead of a secondary battery, establishing a power-autonomous FC system.

B. Verification of the Model

In this section, the model developed in Section II-A is qualitatively confirmed with experiments. The experimental setup consists of a small, commercial FC system (Nexa by Ballard Power System, Inc.), an electric load, and measurement devices installed at the FC Control Laboratory in the University of Michigan. The FC stack system is an example of a power-autonomous FC system supplying power to all its auxiliary components from its own stack power except during start-up and shutdown.

The experimental FC is a fully automated, air-cooled stack system with internal air humidification. The rated net power is 1200 W at full load with the stack voltage at 26 V. The stack has a total of 47 cells connected in series. The FC system has its own dedicated controller and safety systems so the experimental data collected correspond to the closed-loop behavior of the system. An external controllable load was used to test the dynamic behavior of the FC stack.

Sensors were designed and installed to measure the stack voltage, the current of the FC stack and also the auxiliary load current. Two closed-loop hall effect sensors were installed for the net current and auxiliary current measurement. During the experiment, the oxygen excess ratio $\lambda_{\rm O_2}$ was not measured since there was no space for the measurement of air flow rate before the cathode inlet.

Due to the differences in the power between the FC in the model and the FC in the experiment, the experimental validation was performed qualitatively instead of a comparison of the exact measurement. Although the difference in the power range is important, the most important difference in the two systems is the operating pressure. The compressor-driven FC in the model operates at high pressures, whereas the blower-driven FC in the experimental apparatus operates at low pressures. To compare the response of the two systems, the current and voltage load range for the simulation were chosen to achieve relatively low operating pressure and avoid the effect of cathode pressure variations.

The experimental data recorded during a net current change are shown in Fig. 3(a). The net load current increase from 20 to 30 A was applied to the experimental FC at 0.2 s. A pure step change in net current was not applied in order to avoid the

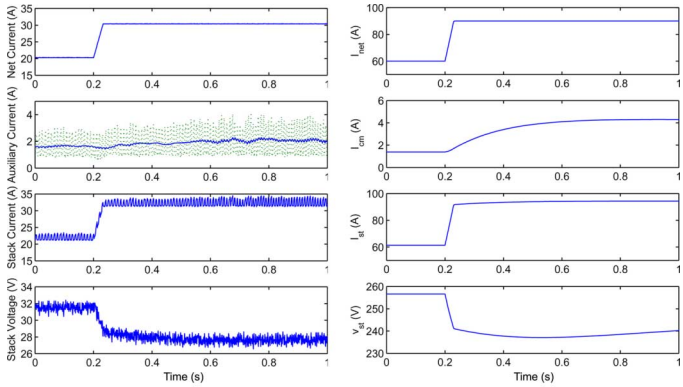

(a) (b)

Fig. 3. Experimental comparison. (a) Experimental results. (b) Simulation result.

effects of the control logic in the electric load and the power cable between the stack and the load. The rate of change of $10/0.02 = 500$ A/s is fast enough to excite the dynamics of the experimental FC. When the net current load increases, the stack voltage immediately drops following the current input. This is followed by a slow voltage decrease that matches the response of the measured auxiliary current, which increases rather slowly, as shown in Fig. 3(a). Due to the slow auxiliary current, we postulated that a filtered feedforward controller similar to the one analyzed in Section V was used by the Nexa control system. The PWM commands to the air supply and the cooling blower and the averaged signal are shown in Fig. 3(a).

Using the model developed in Section II-A, a simulation of a net current change from 60 to 90 A was performed. The air supply control was based on feedforward control from the net current measurement. A first-order filter was added to the feedforward shown in Section V. The filter time constant $\tau_{\rm filter} = 0.4$ s was chosen to match the dynamics of the auxiliary current load. As can be seen in Fig. 3(b), the voltage dynamic behavior of the FC model is similar to the results of the experiment. The changes in the oxygen excess ratio are expected to be as in Fig. 7(b), although this cannot be verified experimentally due to the lack of an OER sensor.

III. Control Problem Formulation for FC Air Supply

The control objective of regulating the oxygen excess ratio $\lambda_{\rm O_2}$ in the FC stack can be achieved by a feedforward and/or feedback control using a compressor motor voltage command $v_{\rm cm}$ during load (current) changes. Since the performance variable $\lambda_{\rm O_2}$ is not directly measured, we regulate $\lambda_{\rm O_2}$ based on two measurements, namely, the demanded load $I_{\rm net}$ and the air flow rate at the compressor $W_{\rm cp}$.

Linear control techniques are used throughout this brief to analyze the inherent control difficulties and to design a controller for the system. A nominal operating point of 40-kW FC net power (67% of the maximum FC net power) is used for the linearization of the nonlinear FC stack system. Deviations from the nominal net current $I^o_{\rm net} = 169$ A, compressor motor voltage command $v^o_{\rm cm} = 164$ V and associated nominal oxygen excess ratio $\lambda^o_{\rm O_2} = 2$ are considered to define the control problem in the general control configuration $[z\ y]^T = G[w\ u]^T$ with

$G = [G_{zw}\ G_{zu};\ G_{yw}\ G_{yu}]$. Specifically, the control of the FC air supply can be described as a disturbance rejection problem with performance variable $z = \delta\lambda_{\mathrm{O}_2} = \lambda_{\mathrm{O}_2} - \lambda^o_{\mathrm{O}_2}$, control input $u = \delta v_{\mathrm{cm}} = v_{\mathrm{cm}} - v^o_{\mathrm{cm}}$, and disturbance input $w = \delta I_{\mathrm{net}} = I_{\mathrm{net}} - I^o_{\mathrm{net}}$.

The plant transfer functions G_{zu} from u to z, and G_{zw} from w to z of the power-autonomous FC are

$$G_{zu} = \frac{-0.00741(s+101)(s-19.2)(s+3.15)(s+3.09)}{(s+71.3)(s+19.6)(s+3.28)(s+3.12)} \quad (7)$$

$$G_{zw} = \frac{-0.0103(s+67.7)(s+19.4)(s+3.29)(s+3.09)}{(s+71.3)(s+19.6)(s+3.28)(s+3.12)}. \quad (8)$$

As can be seen in (7) and (8), G_{zu} and G_{zw} are both stable and have zero relative degrees. The transfer function G_{zw} indicates a minimum phase system, while G_{zu} has a nonminimum phase (NMP) zero $\zeta_z = 19.2$.

The transfer function G_{zu} has a phase lag associated with NMP behavior, whereas G_{zw} resembles a static gain. The flat frequency response of the G_{zw} can be physically explained by the direct effect of the net current I_{net} on the stack current I_{st}, which statically affects the mass flow rate of the oxygen reacted in the cathode $W_{O_2,\mathrm{rct}}$, which, in turn, affects the OER defined by (2). Note that while I_{net} statically affects the $W_{O_2,\mathrm{rct}}$, which is the denominator of OER in (2), it barely affects the cathode pressure p_{ca} (by depleting oxygen) and thus causes insignificant variation in oxygen flow in the cathode $W_{O_2,\mathrm{in}}$, which is the numerator of OER in (2).

The NMP zero in G_{zu} is unavoidable in power-autonomous FC systems. The reason for this is that the actuator u affects the performance variable λ_{O_2} through the flow path and the electrical path (see Fig. 2), with mutual conflicting results. An increase in the compressor command increases the air flow to the FC, and consequently, increases the oxygen excess ratio λ_{O_2}. However, an increase in the compressor command also increases the FC parasitic load I_{cm}, thus, decreasing the oxygen excess ratio. The interaction of these two dynamically different and opposite contributions introduces the NMP behavior. Moreover, it is important that the NMP behavior is always present regardless of the type of compressor or blower in the air supply, as long as the power for the air supply component comes from the stack itself with no energy buffer such as a battery.

Regulation of the oxygen excess ratio can be achieved by a feedforward controller since the disturbance input I_{net} can be measured directly. The design limitations associated with NMP dynamics in G_{zu} and the design of feedforward control are discussed in Sections IV and V.

In addition to the feedforward control, measurements from the plant can be used to improve the performance and/or the robustness. Specifically, a feedback controller based on the compressor flow measurement W_{cp} will be considered in Section VI similar to [5] and [6]. The feedback control can be applied so that W_{cp} tracks the reference air flow command $W^{\mathrm{ref}}_{\mathrm{cp}}$, thus, defining the measurement y

$$y = W^{\mathrm{ref}}_{\mathrm{cp}} - W_{\mathrm{cp}} \quad (9)$$

for the general control configuration. The demanded air flow rate $W^{\mathrm{ref}}_{\mathrm{cp}}$ is based on the stack load measurement I_{st}, and the desired oxygen excess ratio $\lambda^{\mathrm{ref}}_{\mathrm{O}_2}$, as defined in [6]. The linear plant transfer functions G_{yu} and G_{yw} are

$$G_{yu} = \frac{0.198(s-81.9)(s+68.3)(s+3.13)(s+1.07)}{(s+71.3)(s+19.6)(s+3.28)(s+3.12)} \quad (10)$$

$$G_{yw} = \frac{0.274(s+71.9)(s+19.2)(s+3.34)(s+2.9)}{(s+71.3)(s+19.6)(s+3.28)(s+3.12)} \quad (11)$$

for the same operating point defined previously.

The frequency response of G_{yw} resembles a static gain similar to G_{zw}. This flat frequency response is consistent with the system physics because the net load current I_{net} disturbance directly affects $W^{\mathrm{ref}}_{\mathrm{cp}}(I_{\mathrm{st}})$, while causing minor changes in the compressor air flow W_{cp}, in the open-loop plant.

The existence of an NMP zero in G_{yu} is practically unavoidable in a power-autonomous FC system. The control command u affects the measurement $y = W^{\mathrm{ref}}_{\mathrm{cp}}(I_{\mathrm{st}}) - W_{\mathrm{cp}}$ through the flow path and the electric path. Specifically, an increase in the compressor command increases the air flow at the compressor W_{cp}, whereas an increase in the compressor command increase the FC parasitic load I_{cm}, and consequently, the demanded air flow $W^{\mathrm{ref}}_{\mathrm{cp}}(I_{\mathrm{st}})$. The NMP zero $\zeta_y = 81.9$ in the response from u to y imposes feedback bandwidth limitations on the ability to track the air flow requirement $W^{\mathrm{ref}}_{\mathrm{cp}}(I_{\mathrm{st}})$. Therefore, high gain control on the compressor command can cause instabilities when the compressor draws current directly from the stack, which is empirically observed in [5].

The differences in performance z and measurement y introduce more difficulties in the control design. The differences in G_{yu} and G_{zu} characterize the different dynamic behavior of z and y, and thus, the design of the feedback controller using the measurement y needs to take into account the performance variable, i.e., the oxygen excess ratio λ_{O_2}. Prior work in [2]–[4] reports in a qualitative manner that regulating the cathode oxygen flow based on the compressor air flow rate measurement has a potential limitation because the actual air flow at the cathode of the FC stack is not the same as the flow at the compressor, thus causing significant problems in regulating oxygen excess ratio inside the stack. The detailed limitations on feedback control design are covered in Section VI.

IV. Performance Measures and Constraints

While the controller architecture for the FC air supply has already been described in [3], [5] as a combined feedforward and feedback control based on the load current and air flow rate measurement, this brief will first to examine the fundamental limitations of the system. Generalized bounds on control performances are established to clarify and quantify the control difficulties. For performance evaluation, we consider the disturbance response ratio [11]:

$$R_{zw} = \frac{T_{zw}}{G_{zw}} \quad (12)$$

which is the ratio of the closed-loop response T_{zw} to the open-loop response G_{zw}. The disturbance response ratio is a measure of the performance of the controller in rejecting the disturbance

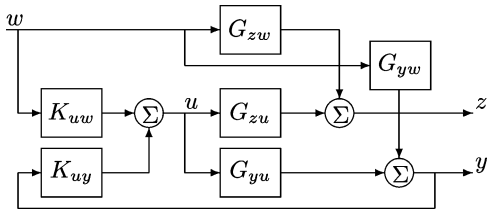

Fig. 4. Control configuration with feedforward/feedback control.

$w = \delta I_{\text{net}}$. Given a feedforward controller K_{uw} and feedback controller K_{uy}, as in Fig. 4, the closed-loop response T_{zw} is

$$T_{zw} = G_{zw} + G_{zu}K_{uw} + G_{zu}K_{uy}(1 - G_{yu}K_{uy})^{-1} \times (G_{yw} + G_{yu}K_{uw}). \quad (13)$$

We consider the integral constraints upon R_{zw} for the control system of the plant (7)–(8) because there exists a NMP zero in G_{zu}. Since the system is open-loop stable, G_{zw} is minimum phase, and G_{zu} has a NMP zero ζ_z, if T_{zw} is minimum phase,[2] then the Poisson integral for NMP zeros of G_{zu} (from Proposition V.7 in [11]) is

$$\int_0^\infty \log|R_{zw}(j\omega)|\, W(\zeta_z, \omega) d\omega = 0 \quad (14)$$

where $W(\zeta_z, \omega) = 2\zeta_z/(\zeta_z^2 + \omega^2)$. Integral constraints upon R_{zw} due to the NMP zero in G_{zu} in (14) dictate that if $|R_{zw}| < 1$ over any frequency range, then necessarily $|R_{zw}| > 1$ at other frequencies since $W(\zeta_z, \omega) > 0, \forall\omega$. Design tradeoffs imposed by the Poisson integral in (14) are valid with arbitrary measurements. Thus, they can be applied with any feedforward and feedback controller.

We also examine the step response of the disturbance response ratio R_{zw} with the normalized integral square output error

$$\left\| \frac{1}{s} R_{zw} \right\|_2^2 \quad (15)$$

and compare the closed-loop performance associated with various controllers using the cost function

$$J_{\lambda_{O_2}} = \int_0^\infty z^2 dt. \quad (16)$$

V. Feedforward Control Design

Since the disturbance input I_{net} is measured, we can apply feedforward control. In the case of a feedforward controller K_{uw} using the disturbance measurement directly as shown in Fig. 4 (without the feedback K_{uy}), the response of z to w is

[2]The existence of NMP zero in T_{zw} cannot be determined without the controller, so the phase of T_{zw} will be confirmed after the control design.

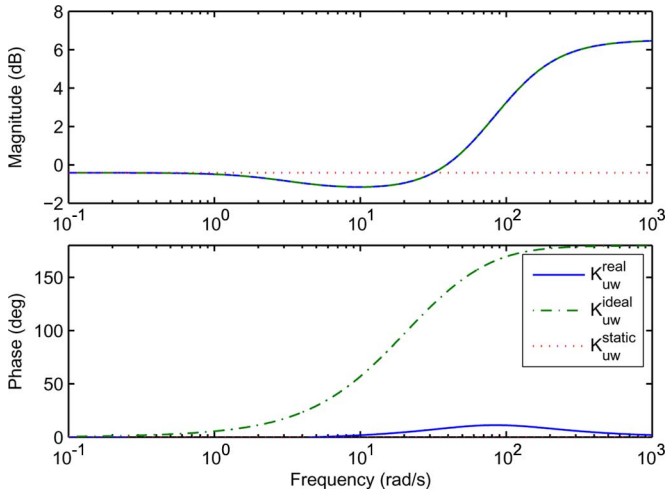

Fig. 5. Frequency responses of the feedforward controllers K_{uw}^{real}, K_{uw}^{ideal}, and K_{uw}^{static}.

TABLE I
Performance Measures $\|(1/s)R_{zw}\|_2^2$ and $J_{\lambda_{O_2}}$ for the Step Disturbance

Controller	$\|\frac{1}{s}R_{zw}\|_2^2$	$J_{\lambda_{O_2}}$
K_{uw}^{real}	0.1044	0.0632
K_{uw}^{static}	0.1051	0.0633
K_{uw}^{static} with $\tau_{filter} = 0.01$	0.1114	0.0650
K_{uw}^{static} with $\tau_{filter} = 0.1$	0.1551	0.0760
K_{uw}^{static} with $\tau_{filter} = 0.4$	0.3008	0.1052

$$T_{zw} = G_{zw} + G_{zu}K_{uw}. \quad (17)$$

Using the performance measures and the insight from the integral constraint in the Section IV, various feedforward controllers are compared and analyzed.

A. Feedforward Cancellation Controller

A cancellation control that perfectly regulates the performance variable z in the presence of measured disturbance w may be achieved with a dynamic feedforward controller based on a plant inversion

$$K_{uw}^{\text{ideal}} = -G_{zu}^{-1}G_{zw}. \quad (18)$$

The resulting cancellation controller K_{uw}^{ideal} is, however, unstable due to the NMP zero ζ_z of G_{zu}. Since perfect disturbance cancellation using feedforward controller K_{uw}^{ideal} is not a robust option, it is necessary to evaluate the disturbance rejection performance of various other feedforward controllers.

B. Dynamic and Static Feedforward Control

A minimum-phase approximation $\tilde{G}_{zu}$ with

$$G_{zu} = \tilde{G}_{zu}\frac{\zeta_z - s}{\zeta_z + s} \quad (19)$$

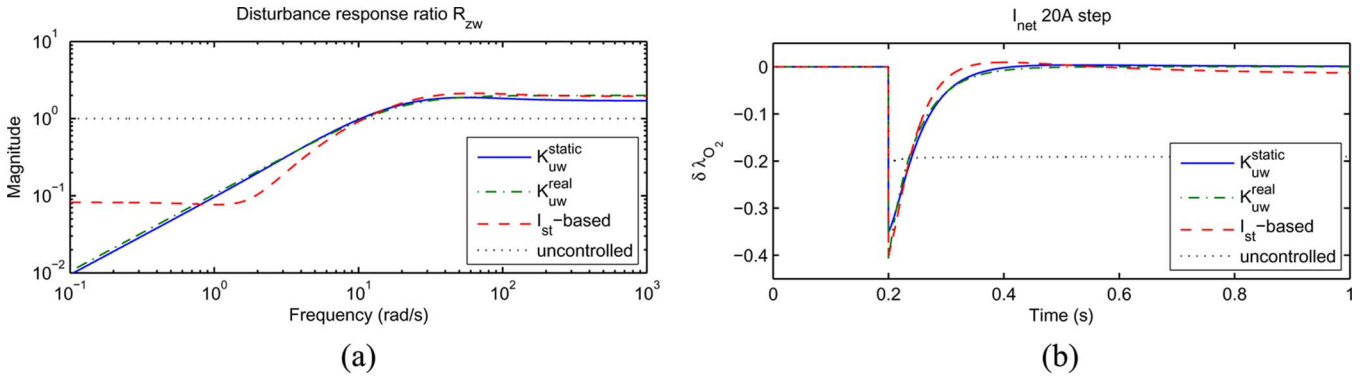

Fig. 6. Disturbance rejection performance with K_{uw}^{real} and K_{uw}^{static} feedforward controller and I_{st}-based controller. (a) Disturbance response ratio. (b) Step response.

can be applied to replace G_{zu} in (18). The transfer function $\tilde{G}_{zu}$ is minimum phase, but maintains the magnitude of G_{zu}. The resulting quasi-cancellation controller K_{uw}^{real} is

$$K_{uw}^{\text{real}} = -\tilde{G}_{zu}^{-1} G_{zw}. \tag{20}$$

The frequency response of the dynamic feedforward controllers K_{uw}^{real} and K_{uw}^{ideal} can be seen in Fig. 5. The magnitudes of the two controller transfer functions are identical, though the phase of K_{uw}^{real} differs by 180° at high-frequency from the phase of K_{uw}^{ideal}.

It is shown in [12] that if G_{zw} is approximated by a static function the feedforward controller, K_{uw}^{real} realizes the minimum achievable normalized integral square output error (using [13, Th. 2]) due to a unit step disturbance

$$\min \left\| \frac{1}{s} R_{zw} \right\|_2^2 = \frac{2}{\zeta_z} = 0.1044. \tag{21}$$

In our case, the load disturbance directly affects the oxygen excess ratio, thus, G_{zw} can be approximated as a static gain indicated by the near pole-zero cancellation in (8). Therefore, it is expected that K_{uw}^{real} can achieve very good disturbance rejection, as indicated by the small values for the measures $\|(1/s)R_{zw}\|_2^2$ and $J_{\lambda_{O_2}}$ in Table I.

We also compare the performance of dynamic feedforward control with a static feedforward controller. The static feedforward controller

$$K_{uw}^{\text{static}} = -\frac{G_{zw}(0)}{G_{zu}(0)} \tag{22}$$

has the desired property that the disturbance is completely rejected at dc. The feedforward controller K_{uw}^{static} is realizable only if the dc gain of G_{zu} is not zero, as is the case for this system. Also, static feedforward control can be easily implemented by a lookup table.

The disturbance response ratios R_{zw} for K_{uw}^{real} and K_{uw}^{static} feedforward control are shown in Fig. 6(a). The closed-loop frequency response of each controller explicitly shows tradeoffs due to the Poisson integral in (14). At low frequency ranges, both controllers perform well with $|R_{zw}| < 1$, while $|R_{zw}| > 1$ at high frequency ranges. The similarity in the disturbance response at low frequency between the dynamic and static feedforward controller can be explained by the frequency response of K_{uw}^{real} and K_{uw}^{static}, as shown in Fig. 5. The magnitude and phase of the dynamic controller K_{uw}^{real} are similar to those of K_{uw}^{static} below the frequency of 10 rad/s. The disturbance response with dynamic feedforward K_{uw}^{real} is slightly larger than that obtained by the static feedforward at high frequency due to the small improvements achieved between 6–40 rad/s.

The disturbance response of both the dynamic and static feedforward controllers to a 20 A step change in load current, corresponding to a power step from 40 to 45 kW, is shown in Fig. 6(b). Both feedforward controllers show similar oxygen excess ratio λ_{O_2} recovery after the initial excursion. The two controllers also achieve similar values for the measures $J_{\lambda_{O_2}}$ and $\|(1/s)R_{zw}\|_2^2$ as shown in Table I. The initial disturbance response following a load step change at 0.2 s shows a larger excursion in oxygen excess ratio with K_{uw}^{real} than that observed with K_{uw}^{static} matching the high frequency behavior in Fig. 6(a).

The initial excursion of λ_{O_2} corresponds to the largest λ_{O_2} deviation from the nominal value, and thus, is the most critical value for oxygen starvation and stack life. This excursion is important enough to warrant further analytic investigation of its value and occurrence. The initial excursion of $z = \delta\lambda_{O_2}$ during a load step change with K_{uw}^{real} can be determined analytically from T_{zw}

$$T_{zw} = G_{zw} + G_{zu} K_{uw}^{\text{real}} = G_{zw} \left(1 - \frac{\zeta_z - s}{\zeta_z + s} \right). \tag{23}$$

The H^∞ norm of R_{zw} with dynamic feedforward control is then

$$\|R_{zw}\|_\infty = \sup_\omega \left| 1 - \frac{\zeta_z - j\omega}{\zeta_z + j\omega} \right| = 2 \tag{24}$$

attained at infinite frequency. This value implies that the disturbance response of dynamic feedforward control is twice as large at high frequencies ($\omega > 100$ rad/s in our problem) as the initial excursion of the uncontrolled plant for a given step disturbance. The ratio $|R_{zw}|_\infty$ is independent of the location of the NMP zero ζ_z and always equals 2 with dynamic feedforward control if there exists an NMP zero in the plant G_{zu}. Since all air flow devices powered directly by the FC cause an NMP behavior in the G_{zu} response, all autonomously powered FC systems will

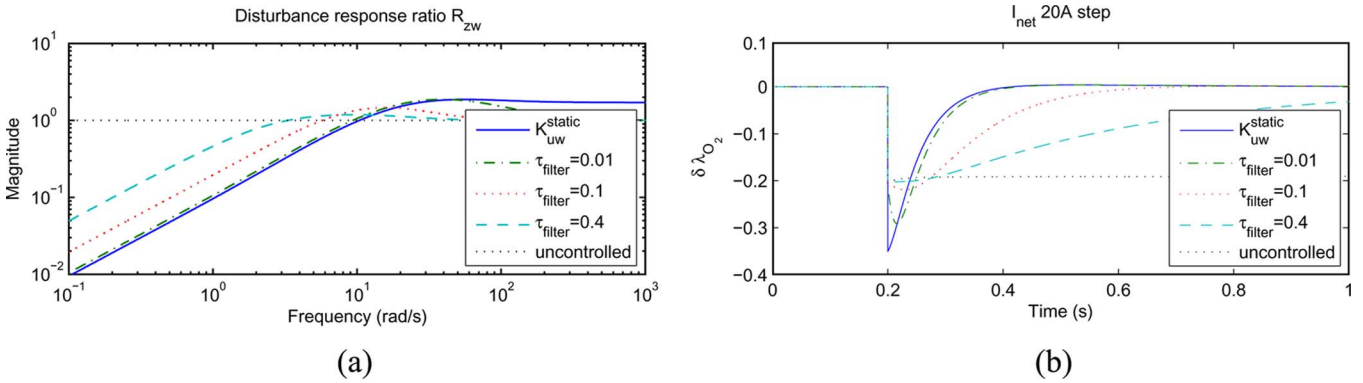

Fig. 7. Disturbance rejection performance of static feedforward with filtered command. (a) Disturbance response ratio. (b) Step response.

thus have a significant drop in oxygen excess ratio response if a similar dynamic feedforward controller is applied.

In the case of the static feedforward controller that exactly cancels the current disturbance at steady state, the initial excursion depends solely on the mismatch between the dynamics from the disturbance to the performance G_{zw} and the dynamics from the control input to the performance G_{zu}. The initial excursion of λ_{O_2} during a load step change with K_{uw}^{static} can be calculated from T_{zw}

$$T_{zw} = G_{zw} + G_{zu}K_{uw}^{\text{static}} = G_{zw} - G_{zu}\frac{G_{zw}(0)}{G_{zu}(0)}. \qquad (25)$$

This time, the H^∞ norm of R_{zw}

$$||R_{zw}||_\infty = \sup_\omega \left|1 - \frac{G_{zu}/G_{zu}(0)}{G_{zw}/G_{zw}(0)}\right| = 1.87 \qquad (26)$$

attained at $\omega = 60$ rad/s, while the infinite frequency response of $|R_{zw}|$ is

$$\lim_{s\to\infty} |R_{zw}| = 1.71. \qquad (27)$$

This corresponds to the initial excursion of the oxygen excess ratio with the static feedforward control K_{uw}^{static}, which is 1.71 times larger than that observed in the uncontrolled plant, as shown in Fig. 6(b). Due to the smaller initial λ_{O_2} excursion and ease of implementation, the static feedforward control K_{uw}^{static} is preferable to the dynamic feedforward control K_{uw}^{real}.

C. I_{st}-Based Controller

Note here that a static feedforward controller which regulates λ_{O_2} at steady state can be implemented by measuring the FC stack current I_{st}, instead of the net (load) current I_{net}. The I_{st}-based feedforward control has been proposed in [6] for the case where the compressor is not powered by the FC stack. When the compressor current is drawn from the FC stack, a portion of the stack load is proportional to the control effort. Therefore, the total stack load current is no longer pure disturbance. Despite the existing algebraic loop, a static map between I_{st} and u can be recorded when simulating the system with the I_{net} based controller.

The disturbance response ratio of the I_{st}-based controller is compared with static feedforward controller in Fig. 6(a). The response with the I_{st}-based control shows larger disturbance amplification than that with K_{uw}^{static} at high frequency ranges (over 10 rad/s). At mid frequency, the disturbance rejection performance is better with I_{st}-based control. This tradeoff between the better mid-frequency response versus the worse high frequency response follows the integral constraints in (14). There is a small dc error with the I_{st}-based controller because linearization is not accurate away from the nominal operating point. The step response in Fig. 6(b) reflects the frequency responses of I_{st}-based control. The initial excursion to a load step using the I_{st}-based controller is larger than that of the static I_{net}-based feedforward controller and recovery time is reduced.

D. Static Feedforward Control With Filtered Command

The NMP zero dynamics of G_{zu} and the associated integral constraints impose a stringent tradeoff between our ability to achieve simultaneously a small initial excursion and a fast recovery of λ_{O_2} for step changes in the load current. A compromise in favor of reducing the initial excursion can be achieved by adding a filter to the static feedforward controller $K_{uw} = K_{uw}^{\text{static}}/(\tau_{\text{filter}} + 1)$.

Integral relations from (14) are still valid even after adding a filter to the controller. The disturbance response ratio in Fig. 7(a) shows the disturbance attenuation over all frequency ranges. The disturbance attenuation at high frequency improves as the time constant of the filter, τ_{filter}, increases. Meanwhile, the disturbance rejection performance at low frequency deteriorates following the Poisson integral constraint in (14).

The step responses in Fig. 7(b) show the tradeoff in the time domain as well. An increased τ_{filter} reduces the amount of initial excursion, but increases the recovery time after the initial excursion occurs. This tradeoff can be analyzed by time-domain integrals. If we have a step disturbance input, $W(s) = w_0/s$, the Laplace transformation of the output is given $Z(s) = G_{zu}U(s) + G_{zw}(w_0/s)$ with

$$Z(\zeta_z) = \int_0^\infty e^{-\zeta_z t} z(t)dt = G_{zw}(\zeta_z)\frac{w_0}{\zeta_z}. \qquad (28)$$

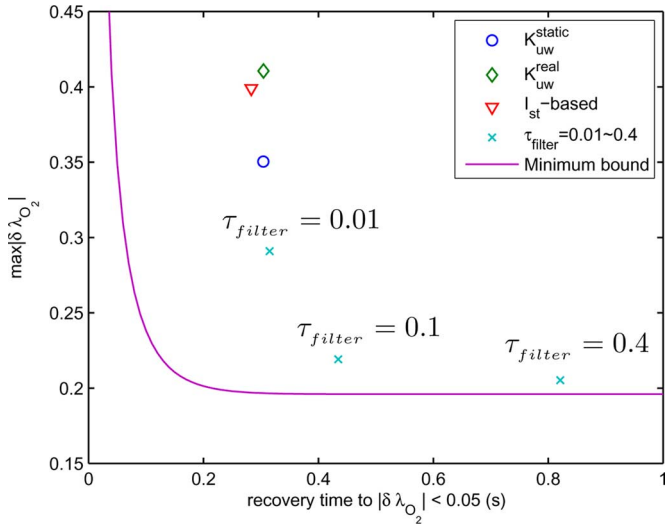

Fig. 8. Oxygen excess ratio excursion versus recovery time comparison.

Splitting the interval of integration at the recovery time, denoted as $t_{\rm rec} = \inf_T\{T : z(t) \geq -0.05 \text{ for } t \in [T,\infty)\}$, it can be shown that

$$\int_0^{t_{\rm rec}} e^{-\zeta_z t} z(t)dt = G_{zw}(\zeta_z)\frac{w_0}{\zeta_z} - \int_{t_{\rm rec}}^{\infty} e^{-\zeta_z t} z(t)dt \qquad (29)$$

and following the proof of Lemma 4 in [14]

$$\max_{t\in(0,t_{\rm rec})} |\delta\lambda_{\rm O_2}| \geq \frac{G_{zw}(\zeta_z)w_0 - 0.05e^{-\zeta_z t_{rec}}}{1-e^{-\zeta_z t_{rec}}}. \qquad (30)$$

Fig. 8 summarizes the tradeoff between the initial excursion and the recovery time of oxygen excess ratio during step disturbances.

The integral square output error $J_{\lambda_{\rm O_2}}$ also increases as $\tau_{\rm filter}$ increases, as shown in Table I. Larger $\tau_{\rm filter}$ increases the recovery time and $J_{\lambda_{\rm O_2}}$ despite the reduced initial excursions. The deterioration in $J_{\lambda_{\rm O_2}}$ can be seen by comparing the areas in Fig. 7(b). The performance measure $\|(1/s)R_{zw}\|_2^2$ is similar to $J_{\lambda_{\rm O_2}}$, as shown in Table I. Although $K_{uw}^{\rm real}$ and $K_{uw}^{\rm static}$ are not necessarily the optimal controllers since G_{uw} is not exactly static, the associated performance is better than that obtained after the filtering.

VI. Feedback Control Design

While the best performance can be achieved with the feedforward control proposed in Section V, feedforward control is sometimes sensitive to uncertainties. Also, cancellation control that perfectly attenuates the disturbance response in the performance variable z may be achieved with a feedback controller. However, the NMP zero ζ_z of G_{zu} does not satisfy the multiplicity bound $m_{zw}(\zeta_z) \geq m_{zu}(\zeta_z) + m_{yw}(\zeta_z)$ that ensures stability from in [11, Prop. IV.6].

The oxygen excess ratio $\lambda_{\rm O_2}$ regulation with feedforward control $K_{uw}^{\rm static}$ or $K_{uw}^{\rm real}$ shows the best integral square output errors from the results in Section V. A simple, proportional and integral (PI) controller $K_{uy} = K_P(1+(K_I/s))$ is added to the static feedforward controller $K_{uw}^{\rm static}$, based on measurements of the difference between $W_{\rm cp}$ and $W_{\rm cp}^{\rm ref}$ in (9), so that a zero steady-state flow error and oxygen excess ratio can be achieved, despite model uncertainties.

The NMP zero ζ_y in G_{yu} affects the closed-loop stability, so that the bandwidth of a stable closed-loop system with feedback control is limited by the NMP zero, e.g., $\omega_{BW,y} < \zeta_y$ [14]. However, this feedback control limitation implies only control bandwidth bounds on regulating the measured output y, and does not necessarily imply degradation in the performance output z because there are differences between the response of G_{zu} and G_{yu}. It is shown in [15] that although high feedback gain improves the tracking of the compressor flow (measurement output y), it deteriorates the regulation of the oxygen excess ratio (performance output). In conclusion, a low gain feedback controller combined with a static feedforward map could provide a control design with adequate performance, robustness, and complexity.

VII. Conclusion

The control design limitations of a power-autonomous FC system are discussed in this brief. A low-order FC system model is introduced to describe the necessary flow and electric dynamics using a combination of physical principles and empirical relations. Experimental comparison is performed using a 1.2-kW 47-cell low-pressure FC stack.

The coupling between the electric and the flow paths in a compressor-driven FC imposes control limitations through NMP zeros in the performance and measurements. The control problem is then formulated in the general control form, and the theory of fundamental limitations is used to clarify the difficulties in avoiding oxygen starvation during load changes. Although the load changes are known (measured), their effects cannot be completely attenuated because NMP zeros make the application of cancellation controllers unfeasible. The design tradeoffs imposed by the Poisson integral associated with the NMP zero are then summarized. Finally, a combined feedforward and feedback control is designed to achieve adequate performance and illustrate the performance limitations in simulation.

References

[1] J. M. Cunningham, M. A. Hoffman, and D. J. Friedman, "A comparison of high-pressure and low-pressure operation of PEM fuel cell systems," SAE Int., Warrendale, PA, 2001-01-0538, 2001.

[2] Y. Motozono, M. Yamashita, M. Yamaoka, K. Nagamiya, and I. Maeda, "Fuel cell control apparatus," U.S. Patent 6 638 652, Oct. 28, 2003.

[3] J. T. Pukrushpan, H. Peng, and A. G. Stefanopoulou, "Control-oriented modeling and analysis for automotive fuel cell systems," *ASME J. Dyn. Syst., Meas., Control*, vol. 126, no. 1, pp. 14–25, 2004.

[4] P. Rodatz, G. Paganelli, and L. Guzzella, "Optimizing air supply control of a PEM fuel cell system," in *Proc. Amer. Control Conf.*, 2003, pp. 2043–2048.

[5] W. Mufford and D. Strasky, "Power control system for a fuel cell powered vehicle," U.S. Patent 5 991 670, Nov. 23, 1999.

[6] J. T. Pukrushpan, A. G. Stefanopoulou, and H. Peng, "Control of fuel cell breathing," *IEEE Control Syst. Mag.*, vol. 24, no. 2, pp. 30–46, Apr. 2004.

[7] G. Boehm, D. P. Wilkinson, S. Khight, R. Schamm, and N. J. Fletcher, "Method and appratus for operating a fuel cell," U.S. Patent 6 461 751, Oct. 8, 2002.

[8] J. T. Pukrushpan, A. G. Stefanopoulou, and H. Peng, *Control of Fuel Cell Power Systems: Principles, Modeling, Analysis and Feedback Design*, ser. Advances in Industrial Control. London, U.K.: Springer-Verlag Telos, 2004.

[9] J. M. Cunningham, M. A. Hoffman, R. M. Moore, and D. J. Friedman, "Requirements for a flexible and realistic air supply model for incorporation into a fuel cell vehicle (FCV) system simulation," SAE Int., Warrendale, PA, 1999-01-2912, 1999.

[10] D. D. Boettner, G. Paganelli, Y. G. Guezennec, G. Rizzoni, and M. J. Moran, "Proton exchange membrane fuel cell system model for automotive vehicle simulation and control," *ASME J. Energy Resources Technol.*, vol. 124, pp. 20–27, 2002.

[11] J. S. Freudenberg, C. V. Hollot, R. H. Middleton, and V. Toochinda, "Fundamental design limitations of the general control configuration," *IEEE Trans. Autom. Control*, vol. 48, no. 8, pp. 1355–1370, Aug. 2003.

[12] G. C. Goodwin, M. E. Salgado, and J. I. Yuz, "Performance limitations for linear feedback systems in the presence of plant uncertainty," *IEEE Trans. Autom. Control*, vol. 48, no. 8, pp. 1312–1319, Aug. 2003.

[13] L. Qui and E. J. Davidson, "Performance limitations of non-minimum phase systems in the servomechanism problem," *Automatica*, vol. 29, no. 2, pp. 337–349, Mar. 1993.

[14] R. H. Middleton, "Trade-offs in linear control system design," *Automatica*, vol. 27, no. 2, pp. 281–292, Mar. 1991.

[15] K.-W. Suh, "Modeling, analysis and control of fuel cell hybrid power systems," Ph.D. dissertation, Mech. Eng. Dept., Univ. Michigan, Ann Arbor, 2006.